

Supporting Information

Large Birefringence Switching in A new Zero-Dimensional Cyanide Perovskite Ferroelastic Material

Jun-Si Zhou,[‡] Luan-Ying Ji,[‡] Shu-Yi Liu, and Xiao-Gang Chen^{*}

Ordered Matter Science Research Center, Nanchang University, Nanchang 330031, People's Republic of China.

E-mail: chenxg@ncu.edu.cn.

Experimental Section

Synthesis of $(MA)_3[Fe(CN)_6]$

All reagents are analytically pure and used without further purification. Iron silver cyanide (10 mmol) and methylamine hydrochloride (30 mmol) were mixed in 10 mL of deionized water at the molar ratio of 1:3 and stirred at room temperature for 30 min. Retain the solution after filtration. After 5 days at room temperature, the red transparent block crystals (Fig. S1a) were obtained by slow solvent evaporation in the mixture.

Differential Scanning Calorimetry (DSC)

Thermal analysis measurements of $(MA)_3[Fe(CN)_6]$ were performed on the Perkin-Elmer Diamond DSC instrument. The powder sample was placed in aluminum crucibles and measured under a nitrogen atmosphere at heating and cooling rates of $20\text{ K}\cdot\text{min}^{-1}$.

Dielectric Measurements

The powder-pressed pellets and crystal of $(MA)_3[Fe(CN)_6]$ coated with silver conducting glue on both sides were used in dielectric measurements. The temperature-dependent dielectric constant was measured on a TH2828A impedance analyzer at 1 MHz with an applied voltage of 1 V.

Single-crystal X-ray Crystallography

Variable-temperature single-crystal X-ray diffraction data were gathered using a Rigaku XtaLAB Synergy-R/DW diffractometer with Cu-K α radiation ($\lambda = 1.54178\text{ \AA}$). Data collection and structural refinement were performed using the Rigaku Crystal Clear and SHELXTL software package. The crystal data and structure refinement of $(MA)_3[Fe(CN)_6]$ are summarized in Table S1. The X-ray crystallographic structures have been deposited at the Cambridge Crystallographic Data Centre (deposition numbers CCDC: 2442254-2442255) and can be obtained free of charge from the CCDC via www.ccdc.cam.ac.uk/getstructures.

Powder X-ray Diffraction (PXRD)

PXRD data were measured on a Rigaku D/MAX 2000 PC X-ray diffractometer with Cu-K α radiation. Diffraction patterns were collected in the 2θ range of $5\text{--}40^\circ$ with a step size of 0.02° . Simulation of the PXRD spectrum was

carried out by the single-crystal data and diffraction-crystal module of the Mercury program.

Raman spectroscopy

Raman spectra were measured by a Raman spectrometer (Horiba, LabRAM HR Evolution) under a 633 nm excitation with the reflection method. The spectrum was dispersed by a 600 groove per millimeter diffraction grating and accumulated 2 times with exposure for 2 s. The temperature dependent Raman spectra were detected by loading the sample in a temperature controller (Linkam, LNP96-S).

Infrared spectroscopy (IR)

IR spectra was measured on a FT-IR Spectrometers (INVENIO R, Bruker) using KBr pellet method. The sample (2 mg) was mixed with KBr (100 mg) and well grounded into powder, and then the mixture was pressed into a thin and transparent sheet for measurement.

Optical microscopy measurements

Ferroelastic domain observations were carried out using an OLYMPUS BX53-P polarizing microscope. For birefringence measurements, the same microscope configuration was employed with the addition of a Berek compensator. The temperature was controlled by a Linkam LTS420 cooling/heating stage with a rate of 10 K/min.

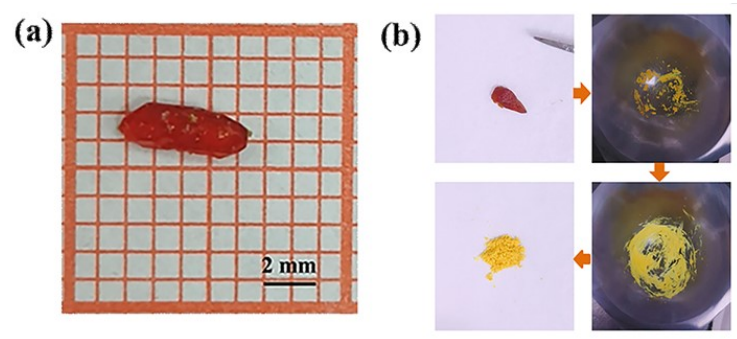


Fig. S1 (a) The crystal of $(MA)_3[Fe(CN)_6]$. (b) Powder preparation via mechanical grinding of $(MA)_3[Fe(CN)_6]$.

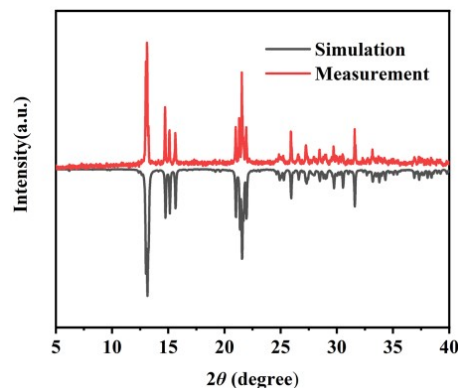


Fig. S2 The experimental PXRD pattern of $(MA)_3[Fe(CN)_6]$ at 298 K matches well with its simulated PXRD pattern.

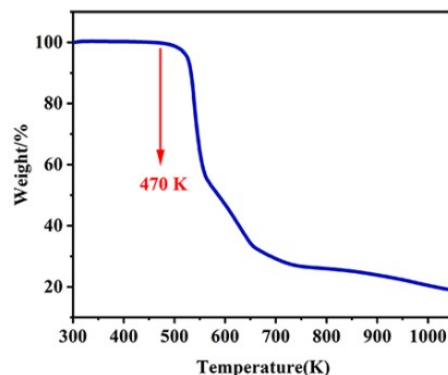


Fig. S3 TGA curves of $(MA)_3[Fe(CN)_6]$.

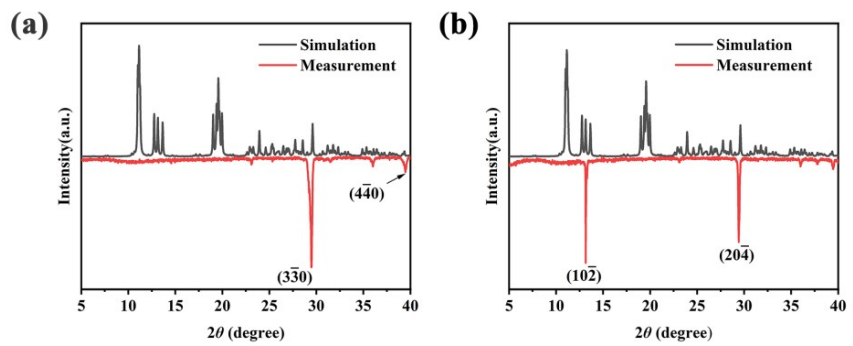


Fig. S4 Measured X-ray diffraction patterns of $(1\bar{1}0)$ plane (a) and $(10\bar{2})$ plane (b) in dielectric measurement and simulated patterns of compounds $(MA)_3[Fe(CN)_6]$.

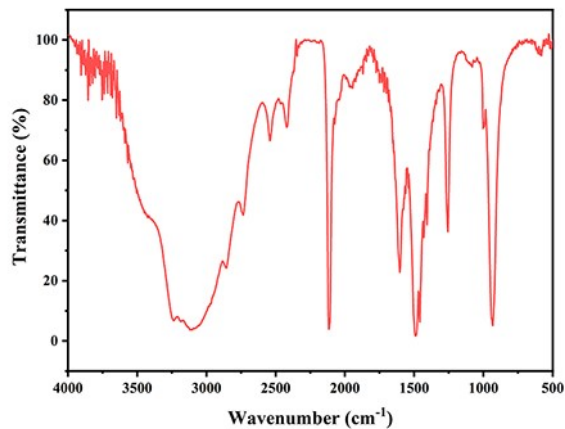


Fig. S5 IR spectra of $(MA)_3[Fe(CN)_6]$ at room temperature.

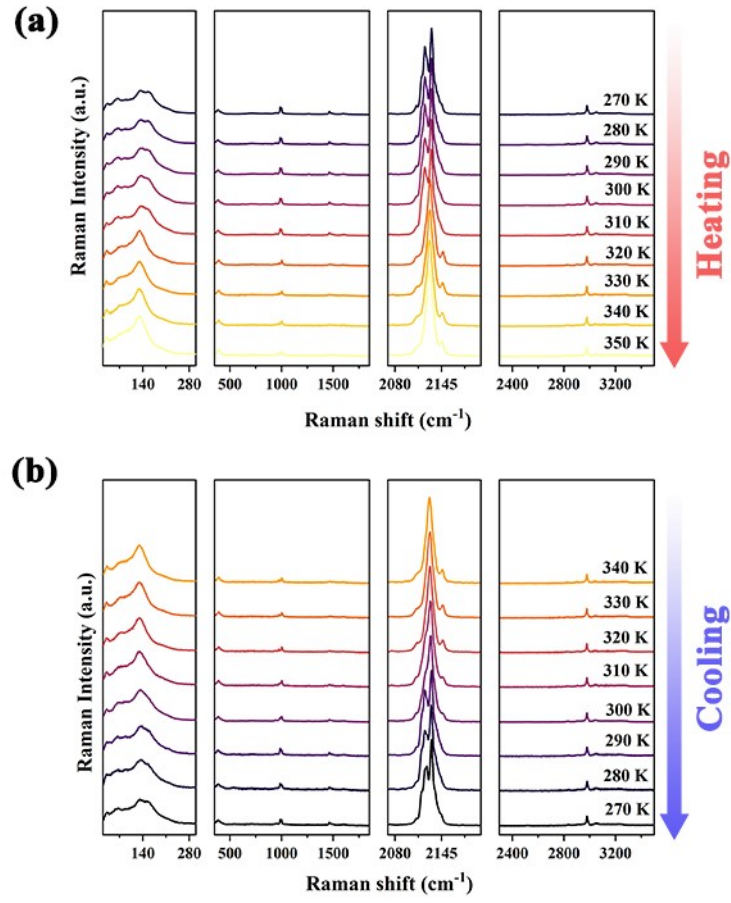


Fig. S6 (a-b) Temperature-dependent Raman spectra of $(MA)_3[Fe(CN)_6]$ in the heating (a) and cooling run (b), respectively.

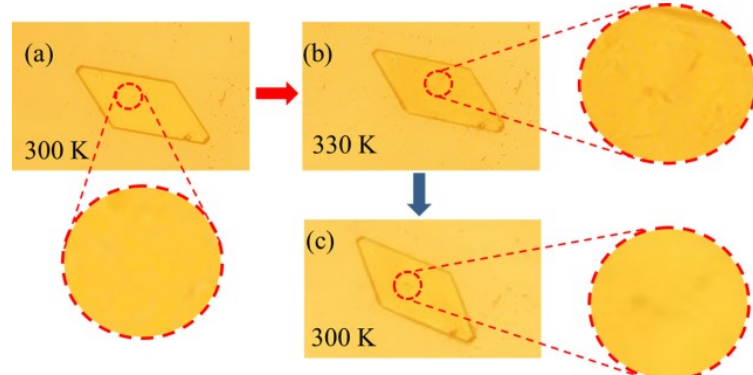


Fig. S7 The change of crystal morphology of $(MA)_3[Fe(CN)_6]$.

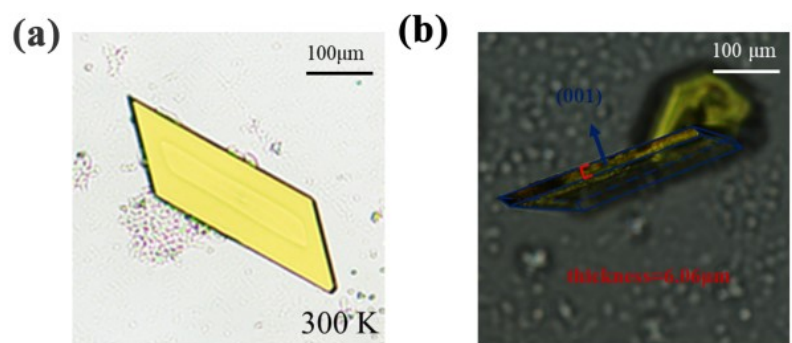


Fig. S8 (a) Single crystal of $(MA)_3[Fe(CN)_6]$ under natural light at 300 K.(b) The thickness of the selected crystal plate for birefringence measurement and the crystal orientation of the selected $(MA)_3[Fe(CN)_6]$ plate determined by single-crystal XRD.

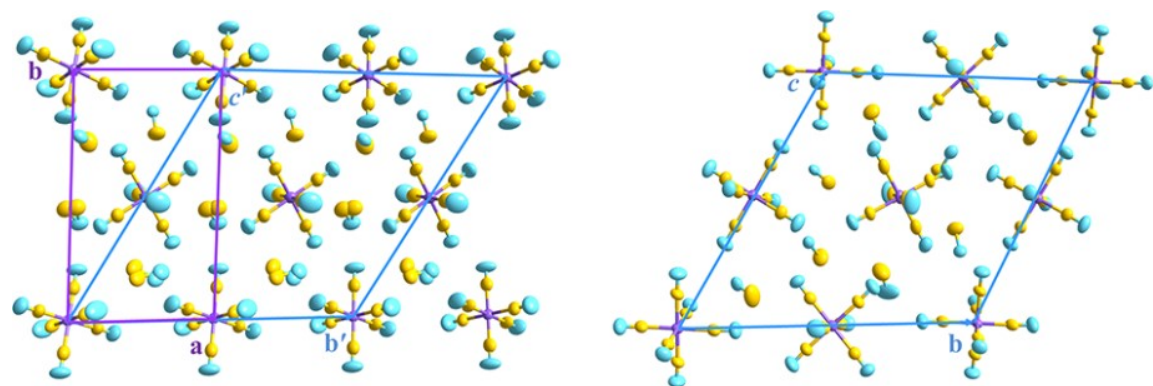


Fig. S9 Transformation of the triclinic HTP lattice (left) to match the unit cell contents of LTP (right).

For the present ferroelastic species, as the cell contents of HTP is different from LTP, a necessary transformation matrix, (0 2 1, 0 0 1, 1 0 0), was applied to the triclinic cell of HTP, giving a transformed cell lattice as, $a' = 14.3096\text{\AA}$, $b' = 16.7192\text{\AA}$, $c' = 16.7558\text{\AA}$, $\alpha' = 58.2434^\circ$, $\beta' = 75.5672^\circ$, $\gamma' = 78.8970^\circ$. As shown in Fig. S9, the unit cell contents of the transformed lattice of HTP matches that of LTP.

Before and after the phase transition, $(\text{MA})_3\text{Fe}(\text{CN})_6$ is located in the triclinic crystal system, and its spontaneous strain tensor is given as:¹

$$[e_{ij}] = \begin{bmatrix} e_{11} & e_{12} & e_{13} \\ 0 & e_{22} & e_{23} \\ 0 & 0 & e_{33} \end{bmatrix}$$

The components of the spontaneous-strain tensor as:

$$e_{11} = \frac{a \sin \gamma}{a_0 \sin \gamma_0} - 1$$

$$e_{22} = \frac{b}{b_0} - 1$$

$$e_{33} = \frac{c \sin \alpha \sin \beta^*}{c_0 \sin \alpha_0 \sin \beta_0^*} - 1$$

$$e_{23} = \frac{1}{2} \left[\frac{c \cos \alpha}{c_0 \sin \alpha_0 \sin \beta_0^*} - \frac{b \cos \alpha_0}{b_0 \sin \alpha_0 \sin \beta_0^*} + \frac{\cos \beta_0^*}{\sin \beta_0^* \sin \gamma_0} \left(\frac{a \cos \gamma}{a_0} - \frac{b \cos \gamma_0}{b_0} \right) \right]$$

$$e_{13} = \frac{1}{2} \left(\frac{a \sin \gamma \cos \beta_0^*}{a_0 \sin \gamma_0 \sin \beta_0^*} - \frac{c \sin \alpha \cos \beta^*}{c_0 \sin \alpha_0 \sin \beta_0^*} \right)$$

$$e_{12} = \frac{1}{2} \left(\frac{a \cos \gamma}{a_0 \sin \gamma_0} - \frac{b \cos \gamma_0}{b_0 \sin \gamma_0} \right)$$

In these equations a , b , c , α , β^* , and γ refer to the low-symmetry form at a given temperature (and pressure), and a_0 , b_0 , c_0 , α_0 , β_0^* , and γ_0 are the cell parameters that the high-symmetry form would possess at the same temperature (and pressure) had the transition not taken place, β^* and β_0^* are reciprocal lattice angles.

The phase transition brings about a total ε_{ss} of

$$\varepsilon_{ss} = \sqrt{\sum_{ij} e_{ij}^2} = 0.1063$$

Table S1. Crystal data and structure refinement of $(MA)_3[Fe(CN)_6]$ at 300 K, and 360 K.

Compound	$(MA)_3[Fe(CN)_6]$	
Temperature	300 K	360 K
Phase	LTP	HTP
Formula	$C_9H_{18}FeN_9$	$C_9H_{18}FeN_9$
Formula weight	308.17	308.17
Crystal system	triclinic	triclinic
Space group	$P\bar{1}$	$P\bar{1}$
$a/\text{\AA}$	14.0643(4)	8.3596(6)
$b/\text{\AA}$	16.3738(5)	14.2547(8)
$c/\text{\AA}$	16.5138(8)	14.3096(8)
$\alpha/^\circ$	60.714(4)	81.942(5)
$\beta/^\circ$	76.502(3)	74.897(5)
$\gamma/^\circ$	75.116(3)	88.154(5)
Volume/ \AA^3	3179.3(2)	1630.01(18)
Z	8	4
Density/ $\text{g}\cdot\text{cm}^{-3}$	1.288	1.256
R_1	0.0865	0.1190
wR_2	0.1783	0.2834
GOF	1.067	1.072

Table S2. Bond Lengths for $(MA)_3[Fe(CN)_6]$ at 300K, and 360 K.

Temperatur	Atom	Atom	Length/Å	Atom	Atom	Length/Å
300 K	Fe1	C1	1.935(6)	N1	C1	1.151(6)
	Fe1	C1 ¹	1.935(6)	N2	C2	1.142(7)
	Fe1	C2 ¹	1.930(6)	N3	C3	1.153(7)
	Fe1	C2	1.930(6)	N4	C4	1.142(6)
	Fe1	C3	1.948(6)	N5	C5	1.151(7)
	Fe1	C3 ¹	1.948(6)	N6	C6	1.144(6)
	Fe2	C4 ²	1.949(6)	N7	C7	1.154(7)
	Fe2	C4	1.949(6)	N8	C8	1.147(7)
	Fe2	C5	1.942(6)	N9	C9	1.147(7)
	Fe2	C5 ²	1.942(6)	N10	C10	1.130(7)
	Fe2	C6 ²	1.934(6)	N11	C11	1.146(7)
	Fe2	C6	1.934(6)	N12	C12	1.129(7)
	Fe3	C7 ³	1.922(6)	N13	C13	1.139(7)
	Fe3	C7	1.922(6)	N14	C14	1.145(7)
	Fe3	C8 ³	1.934(6)	N15	C15	1.136(7)
	Fe3	C8	1.934(6)	N16	C16	1.115(7)
	Fe3	C9	1.937(6)	N17	C17	1.145(7)
	Fe3	C9 ³	1.937(6)	N18	C18	1.137(7)
	Fe4	C10	1.942(6)	N19	C19	1.144(7)
	Fe4	C10 ⁴	1.942(6)	N20	C20	1.156(7)
	Fe4	C11	1.935(7)	N21	C21	1.152(6)
	Fe4	C11 ⁴	1.935(7)	N22	C22	1.140(7)
	Fe4	C12 ⁴	1.930(6)	N23	C23	1.134(7)
	Fe4	C12	1.930(6)	N24	C24	1.148(7)
	Fe5	C13	1.960(6)	N25	C25	1.373(8)
	Fe5	C14	1.951(7)	N26	C26	1.433(7)
	Fe5	C15	1.949(6)	N27	C27	1.455(7)
	Fe5	C16	1.947(6)	N28	C28	1.424(8)
	Fe5	C17	1.927(7)	N29	C29	1.398(8)
	Fe5	C18	1.938(6)	N30	C30	1.459(7)
	Fe6	C19	1.944(6)	N31	C31	1.444(7)
	Fe6	C20	1.927(6)	N32	C32	1.446(9)
	Fe6	C21	1.923(6)	N33	C33	1.433(8)
	Fe6	C22	1.955(6)	N34	C34	1.412(8)
	Fe6	C23	1.952(7)	N35	C35	1.379(7)
	Fe6	C24	1.936(6)	N36	C36	1.419(8)
360 K	Fe1	C1	1.939(10)	N3	C3	1.139(12)
	Fe1	C1 ⁵	1.939(10)	N4	C4	1.137(13)
	Fe1	C2	1.923(12)	N5	C5	1.127(14)
	Fe1	C2 ⁵	1.923(12)	N6	C6	1.128(13)

Fe1	C3	1.922(11)	N7	C7	1.123(14)
Fe1	C3 ⁵	1.922(11)	N8	C8	1.130(14)
Fe2	C4	1.942(11)	N9	C9	1.119(14)
Fe2	C5	1.922(12)	N10	C10	1.144(12)
Fe2	C6	1.947(10)	N11	C11	1.135(12)
Fe2	C7	1.911(11)	N12	C12	1.121(14)
Fe2	C8	1.919(12)	N13B	C13A	1.444(19)
Fe2	C9	1.924(11)	N14	C14	1.438(11)
Fe3	C10 ⁶	1.943(11)	N15	C15B	1.416(18)
Fe3	C10	1.943(10)	N15	C15A	1.417(17)
Fe3	C11 ⁶	1.950(10)	N16	C16B	1.402(17)
Fe3	C11	1.950(10)	N16	C16A	1.410(18)
Fe3	C12 ⁶	1.916(12)	N17B	C17B	1.450(19)
Fe3	C12	1.916(12)	N18	C18	1.440(10)
N1	C1	1.133(11)	C13B	N13A	1.465(19)
N2	C2	1.147(14)	N17A	C17A	1.41(2)

Symmetry code(s): ¹1-X,-Y,1-Z; ²1-X,1-Y,1-Z; ³1-X,1-Y,2-Z; ⁴1-X,2-Y,2-Z; ⁵1-X,1-Y,1-Z; ⁶2-X,2-Y,1-Z

Table S3. Bond Angles for (MA)₃[Fe(CN)₆] at 300K, and 360 K.

Temperature	Atom	Atom	Atom	Angle/ [°]	Atom	Atom	Atom	Angle/ [°]
300 K	C1 ¹	Fe1	C1	180.0	C12 ⁴	Fe4	C11	92.4(3)
	C1 ¹	Fe1	C3 ¹	88.4(2)	C12 ⁴	Fe4	C11 ⁴	87.6(3)
	C1 ¹	Fe1	C3	91.6(2)	C12 ⁴	Fe4	C12	180.0
	C1	Fe1	C3	88.4(2)	C14	Fe5	C13	89.5(2)
	C1	Fe1	C3 ¹	91.6(2)	C15	Fe5	C13	88.3(2)
	C2	Fe1	C1	90.8(2)	C15	Fe5	C14	93.0(3)
	C2	Fe1	C1 ¹	89.2(2)	C16	Fe5	C13	178.5(2)
	C2 ¹	Fe1	C1 ¹	90.8(2)	C16	Fe5	C14	89.4(3)
	C2 ¹	Fe1	C1	89.2(2)	C16	Fe5	C15	90.7(2)
	C2 ¹	Fe1	C2	180.0	C17	Fe5	C13	90.1(2)
	C2	Fe1	C3	91.8(2)	C17	Fe5	C14	178.1(3)
	C2	Fe1	C3 ¹	88.2(2)	C17	Fe5	C15	88.9(3)
	C2 ¹	Fe1	C3 ¹	91.8(2)	C17	Fe5	C16	91.0(3)
	C2 ¹	Fe1	C3	88.2(2)	C17	Fe5	C18	89.0(3)
	C3	Fe1	C3 ¹	180.0	C18	Fe5	C13	93.8(2)
	C4	Fe2	C4 ²	180.0	C18	Fe5	C14	89.2(3)
	C5 ²	Fe2	C4 ²	88.0(2)	C18	Fe5	C15	177.0(2)
	C5	Fe2	C4	88.0(2)	C18	Fe5	C16	87.2(2)
	C5 ²	Fe2	C4	92.0(2)	C19	Fe6	C22	177.7(2)
	C5	Fe2	C4 ²	92.0(2)	C19	Fe6	C23	87.8(2)
	C5 ²	Fe2	C5 ²	180.00(12)	C20	Fe6	C19	90.5(2)
	C6	Fe2	C4	89.2(2)	C20	Fe6	C22	91.8(2)
	C6 ²	Fe2	C4	90.8(2)	C20	Fe6	C23	177.7(3)
	C6 ²	Fe2	C4 ²	89.2(2)	C20	Fe6	C24	89.7(3)

	C6	Fe2	C4 ²	90.8(2)	C21	Fe6	C19	93.6(2)
	C6 ²	Fe2	C5 ²	91.9(2)	C21	Fe6	C20	87.8(2)
	C6	Fe2	C5 ²	88.1(2)	C21	Fe6	C22	86.6(2)
	C6 ²	Fe2	C5	88.1(2)	C21	Fe6	C23	90.7(2)
	C6	Fe2	C5	91.9(2)	C21	Fe6	C24	177.3(2)
	C6	Fe2	C6 ²	180.0	C23	Fe6	C22	89.8(2)
	C7 ³	Fe3	C7	180.0(5)	C24	Fe6	C19	87.7(2)
	C7 ³	Fe3	C8	87.6(2)	C24	Fe6	C22	92.3(2)
	C7 ³	Fe3	C8 ³	92.4(2)	C24	Fe6	C23	91.7(3)
	C7	Fe3	C8 ³	87.6(2)	N1	C1	Fe1	178.0(6)
	C7	Fe3	C8	92.4(2)	N2	C2	Fe1	179.9(8)
	C7	Fe3	C9 ³	86.9(3)	N3	C3	Fe1	178.7(6)
	C7 ³	Fe3	C9	86.9(3)	N4	C4	Fe2	177.8(5)
	C7	Fe3	C9	93.1(3)	N5	C5	Fe2	177.4(6)
	C7 ³	Fe3	C9 ³	93.1(3)	N6	C6	Fe2	177.4(6)
	C8 ³	Fe3	C8	180.0(4)	N7	C7	Fe3	176.6(6)
	C8 ³	Fe3	C9	88.9(3)	N8	C8	Fe3	176.4(6)
	C8	Fe3	C9	91.1(3)	N9	C9	Fe3	176.1(6)
	C8 ³	Fe3	C9 ³	91.1(3)	N10	C10	Fe4	178.1(6)
	C8	Fe3	C9 ³	88.9(3)	N11	C11	Fe4	176.5(6)
	C9 ³	Fe3	C9	180.0	N12	C12	Fe4	175.7(7)
	C10	Fe4	C10 ⁴	180.0	N13	C13	Fe5	177.5(5)
	C11 ⁴	Fe4	C10	90.3(3)	N14	C14	Fe5	179.6(7)
	C11	Fe4	C10	89.7(3)	N15	C15	Fe5	177.9(7)
	C11 ⁴	Fe4	C10 ⁴	89.7(3)	N16	C16	Fe5	178.2(6)
	C11	Fe4	C10 ⁴	90.3(3)	N17	C17	Fe5	175.9(6)
	C11	Fe4	C11 ⁴	180.0	N18	C18	Fe5	177.3(6)
	C12 ⁴	Fe4	C10	88.5(3)	N19	C19	Fe6	175.9(6)
	C12	Fe4	C10 ⁴	88.5(3)	N20	C20	Fe6	178.1(6)
	C12 ⁴	Fe4	C10 ⁴	91.5(3)	N21	C21	Fe6	176.1(5)
	C12	Fe4	C10	91.5(3)	N22	C22	Fe6	177.4(6)
	C12	Fe4	C11 ⁴	92.4(3)	N23	C23	Fe6	177.0(6)
	C12	Fe4	C11	87.6(3)	N24	C24	Fe6	177.9(6)
360 K	C1 ⁵	Fe1	C1	180.0	C9	Fe2	C6	179.1(6)
	C2 ⁵	Fe1	C1	89.9(5)	C10 ⁶	Fe3	C10	180.0
	C2	Fe1	C1	90.1(5)	C10 ⁶	Fe3	C11	89.9(4)
	C2 ⁵	Fe1	C1 ⁵	90.1(5)	C10 ⁶	Fe3	C11 ⁶	90.1(4)
	C2	Fe1	C1 ⁵	89.9(5)	C10	Fe3	C11 ⁶	89.9(4)
	C2 ⁵	Fe1	C2	180.00(6)	C10	Fe3	C11	90.1(4)
	C3 ⁵	Fe1	C1	88.2(4)	C11 ⁶	Fe3	C11	180.0
	C3	Fe1	C1 ⁵	88.2(4)	C12 ⁶	Fe3	C10 ⁶	88.0(4)
	C3 ⁵	Fe1	C1 ⁵	91.8(4)	C12	Fe3	C10 ⁶	92.0(4)
	C3	Fe1	C1	91.8(4)	C12 ⁶	Fe3	C10	92.0(4)
	C3	Fe1	C2 ⁵	91.3(5)	C12	Fe3	C10	88.0(4)

C3 ⁵	Fe1	C2 ⁵	88.7(5)	C12 ⁶	Fe3	C11	91.5(5)
C3 ⁵	Fe1	C2	91.3(5)	C12	Fe3	C11	88.5(5)
C3	Fe1	C2	88.7(5)	C12 ⁶	Fe3	C11 ⁶	88.5(5)
C3 ⁵	Fe1	C3	180.0	C12	Fe3	C11 ⁶	91.5(5)
C4	Fe2	C6	93.5(5)	C12 ⁶	Fe3	C12	180.0
C5	Fe2	C4	89.8(5)	N1	C1	Fe1	179.7(10)
C5	Fe2	C6	92.3(5)	N2	C2	Fe1	178.1(12)
C5	Fe2	C9	88.7(6)	N3	C3	Fe1	177.5(12)
C7	Fe2	C4	176.5(5)	N4	C4	Fe2	176.6(11)
C7	Fe2	C5	88.0(5)	N5	C5	Fe2	178.6(12)
C7	Fe2	C6	89.3(5)	N6	C6	Fe2	176.3(11)
C7	Fe2	C8	89.2(5)	N7	C7	Fe2	178.9(13)
C7	Fe2	C9	90.9(5)	N8	C8	Fe2	176.1(12)
C8	Fe2	C4	92.9(5)	N9	C9	Fe2	176.7(14)
C8	Fe2	C5	176.9(5)	N10	C10	Fe3	179.0(11)
C8	Fe2	C6	89.1(5)	N11	C11	Fe3	179.3(12)
C8	Fe2	C9	90.0(6)	N12	C12	Fe3	179.1(14)
C9	Fe2	C4	86.4(5)				

Symmetry code(s): ¹1-X,-Y,1-Z; ²1-X,1-Y,1-Z; ³1-X,1-Y,2-Z; ⁴1-X,2-Y,2-Z; ⁵1-X,1-Y,1-Z; ⁶2-X,2-Y,1-Z

Table S4. The hydrogen bonds of (MA)₃[Fe(CN)₆] at 300 K.

Temperature	D	H	A	d(D-H)/Å	d(H-A)/Å	d(D-A)/Å	D-H-A/°
300 K	N25	H25B	N21	0.89	2.06	2.921(7)	161.2
	N25	H25C	N2	0.89	2.11	2.885(7)	145.0
	N28	H28B	N8	0.89	2.08	2.859(8)	146.1
	N30	H30B	N11	0.89	2.08	2.900(8)	152.3
	N31	H31B	N10	0.89	2.01	2.833(7)	153.3
	N31	H31C	N7	0.89	2.04	2.872(7)	155.9
	N32	H32A	N14	0.89	2.09	2.901(8)	151.1
	N34	H34A	N24	0.89	2.01	2.882(7)	167.3
	N36	H36C	N12	0.89	1.89	2.768(8)	168.8

Table S5. Organic-inorganic hybrid birefringence crystals.

Compound	birefringence	Ref
(C ₅ N ₁₀ H ₁₀) ₂ PbI ₇ ·H ₂ O	0.49@550 nm	²
[C ₃ N ₆ H ₇] ₂ [B ₃ O ₃ F ₄ (OH)]	0.440@546 nm	³
C(NH ₂) ₃ MoO ₃ (IO ₃)	0.426 @546 nm	⁴
(C ₆ N ₁₀ H ₈)Pb ₂ Br ₆	0.42@550 nm	⁵
Zn(C ₆ H ₄ NO ₂) ₂ ·4H ₂ O	0.37@550 nm	⁶
(C ₆ H ₅ N ₂)HgCl ₃	0.360@546nm	⁷
C ₃ N ₆ H ₇ SO ₃ NH ₂	0.340@546 nm	⁸
MLAPbBr ₄ (MLA=melamine)	0.322@550 nm	⁹
(MA) ₃ Fe(CN) ₆	0.302@546 nm	This work
MLASnCl ₄ (MLA = melamine)	0.294@550 nm	¹⁰
(C ₆ H ₆ NO ₂) (H ₂ PO ₄)	0.284@546 nm	¹¹
(C ₅ H ₆ ON) ₂ [Sb ₂ O(C ₂ O ₄) ₃]	0.279@ 546 nm	¹²
(C ₃ N ₆ H ₆) ₄ HPF ₆	0.264@ 546 nm	¹³
C ₅ H ₁₄ Br ₅ N ₂ Sb	0.262@510 nm	¹⁴
Rb ₂ MoO ₂ (I ₂ O ₆)(IO ₃) ₂	0.261 @546 nm	⁴
TiO ₂	0.256@546 nm	¹⁵
(C ₃ N ₂ I ₂ H ₃) ₂ Mo ₂ O ₅ (IO ₃) ₄ ·4H ₂ O	0.254@ 550 nm	¹⁶
(C ₃ N ₆ H ₆) ₂ (C ₃ N ₆ H ₇)PF ₆ H ₂ O	0.243@546 nm	¹³
C ₄ N ₃ H ₆ SO ₃ NH ₂	0.233@546 nm	¹⁷
(C ₄ H ₆ N ₃)(H ₂ PO ₃)	0.225@589.3 nm	¹⁸
(C ₆ H ₅ N ₂) ₂ ZnCl ₄	0.22@546 nm	¹⁹
YVO ₄	0.204@532 nm	²⁰
[C(NH ₂) ₃] ₆ Mo ₇ O ₂₄	0.203@550 nm	²¹
(C ₃ H ₅ N ₂)SbF ₂ SO ₄	0.193@546 nm	²²
(C ₅ H ₆ N)SbF ₂ SO ₄	0.179@546 nm	²²
CaCO ₃	0.172@532 nm	²³
(C ₁₀ N ₂ H ₁₀)(HI ₂ O ₆)(HIO ₃)(IO ₃)	0.171 @550 nm	²⁴
[C ₈ H ₆ BrN ₂ O]Cl	0.169@550nm	²⁵
[C(NH ₂) ₃] ₁₀ (MoO ₃) ₁₀ (PO ₄) ₂ (HPO ₄) ₂ ·5H ₂ O	0.158@550 nm	²⁶
(C ₅ H ₆ N) ₂ B ₂ O(HPO ₄) ₂ (4PBP)	0.156 @ 546 nm	²⁷
[C(NH ₂) ₃]SbFPO ₄ ·H ₂ O	0.151@546 nm	²⁸
[C(NH ₂) ₃] ₂ S ₂ O ₆	0.150 @546 nm	²⁹
[C ₈ H ₆ IN ₂ O]Cl	0.145@550 nm	²⁵
[C(NH ₂) ₃]BiCl ₂ SO ₄	0.143@546 nm	³⁰
(C ₃ N ₂ H ₅) ₂ Mo ₂ O ₅ (IO ₃) ₄ ·3H ₂ O	0.143 @ 550 nm	¹⁶

(CN ₄ H ₇)SbC ₂ O ₄ F ₂ (H ₂ O) _{0.5}	0.126@546 nm	³¹
α -BaB ₂ O ₄	0.122@546 nm	³²
C ₅ H ₁₄ N ₂ Cl ₅ Sb	0.104@510 nm	¹⁴
(C ₉ H ₁₄ N)SbCl ₄	0.095@546 nm	³³
(C ₈ H ₆ BrN ₂ O)NO ₃	0.08@550 nm	³⁴
LiNbO ₃	0.074@546 nm	³⁵
[C(NH ₂) ₃] ₂ Sb ₃ F ₃ (HPO ₃) ₄	0.027@546 nm	²⁸

References:

1. M. A. Carpenter, E. K. H. Salje and A. Graeme-Barber, Spontaneous strain as a determinant of thermodynamic properties for phase transitions in minerals, *Eur. J. Mineral.*, 1998, **10**, 621-691.
2. W. Huang, X. Song, Y. Li, Y. Zhou, Q. Xu, Y. Song, H. Wang, M. Li, S. Zhao and J. Luo, Designing a Hybrid Perovskite with Enlarged Birefringence and Bandgap for Modulation of Light Polarization, *Small*, 2024, **20**, 2306158.
3. C. Jin, F. Li, Z. Yang, S. Pan and M. Mutailipu, $[C_3N_6H_7]_2[B_3O_3F_4(OH)]$: a new hybrid birefringent crystal with strong optical anisotropy induced by mixed functional units, *J. Mater. Chem. C*, 2022, **10**, 6590-6595.
4. W. Zeng, Y. Tian, X. Dong, L. Huang, H. Zeng, Z. Lin and G. Zou, $C(NH_2)_3MoO_3(I_0_3)$: A Molybdenyl Iodate with Giant Birefringence Designed via a Cation–Anion Synergetic Interaction Strategy, *Chem. Mater.*, 2024, **36**, 2138-2146.
5. Q. Xu, W. Huang, H. Wang, Y. Li, Y. Zhou, L. Hou, S. Zhao and J. Luo, Designing a Dimension Reduced Hybrid Perovskite with Robust Large Birefringence by Expanding Cationic π -Delocation, *Small*, 2023, **19**, 2304333.
6. Y. Shen, Y. Wang, Z. Chen and W. Lu, $Zn(C_6H_4NO_2)_2 \cdot 4H_2O$: A Solar-Blind Birefringent Crystal, *Cryst. Growth Des.*, 2024, **24**, 4288-4292.
7. R.-L. Tang, D.-X. Yang, L. Ma, Y.-L. Lv, W. Liu and S.-P. Guo, $(C_6H_5N_2)HgCl_3$: Discovery of a Polar Hg-Based Hybrid Halide as Preeminent Nonlinear Optical and Birefringent Material Activated by π -Conjugated Organic Cation Substitution, *Adv. Optical Mater.*, 2024, 2403044.
8. D. Dou, Q. Shi, Y. Bai, C. Chen, B. Zhang and Y. Wang, $C_3N_6H_7SO_3NH_2$: non- π -conjugated tetrahedra decoupling π -conjugated groups achieving large optical anisotropy and wide band gap, *Mater. Chem. Front.*, 2023, **7**, 5924-5931.
9. W. Huang, X. Zhang, Y. Li, Y. Zhou, X. Chen, X. Li, F. Wu, M. Hong, J. Luo and S. Zhao, A Hybrid Halide Perovskite Birefringent Crystal, *Angew. Chem. Int. Ed.*, 2022, **61**, e202202746.
10. W. Huang, X. Wu, B. Ahmed, Y. Li, Y. Zhou, H. Wang, Y. Song, X. Kuang, J. Luo and S. Zhao, A hybrid halide lead-free pseudo-perovskite with large birefringence, *Inorg. Chem. Front.*, 2023, **10**, 2039-2044.
11. M.-B. Xu, J. Chen, H.-Y. Wu, J.-J. Li, N. Yu, M.-F. Zhuo, F.-F. Mao and K.-Z. Du, Designing promising ultraviolet (UV) birefringent crystals with different hydrogen-bonded phosphate frameworks, *Inorg. Chem. Front.*, 2024, **11**, 4307-4317.
12. D.-X. Jiao, H.-L. Zhang, C. He, S.-Y. Chen, K. Wang, X.-H. Zhang, L. Wei and Q. Wei, Layered $(C_5H_6ON)_2[Sb_2O(C_2O_4)_3]$ with a large birefringence derived from the uniform arrangement of π -conjugated units, *Chin. J. Struct. Chem.*, 2024, **43**, 100304.
13. L. Liu, F. Yuan, Y. Huang, Z. Lin and L. Zhang, Two UV optical crystals with strong optical anisotropy, large band gaps and an α -BBO type structure, *Dalton Trans.*, 2023, **52**, 5798-5803.
14. S. Qi, P. Cheng, X. Han, F. Ge, R. Shi, L. Xu, G. Li and J. Xu, Organic-Inorganic Hybrid Antimony(III) Halides for Second Harmonic Generation, *Cryst. Growth Des.*, 2022, **22**, 6545-6553.
15. J. R. DeVore, Refractive Indices of Rutile and Sphalerite, *J. Opt. Soc. Am.*, 1951, **41**, 416-419.
16. J.-J. Zhao, S.-F. Li, M.-H. Lv, J.-X. Wang, R.-L. Tang, H. Huang, B. Zhang and D. Yan, Cationic Modification in Hybrid Iodates: A Pathway to Superior Performance, *Inorg. Chem.*, 2025, **64**, 807-812.
17. D. Dou, Q. Shi, H. Li, B. Zhang, D. Yang and Y. Wang, Rational Combination of π -Conjugated and Non- π -Conjugated Groups Achieving Strong Nonlinear Optical Response, Large Optical Anisotropy, and UV Light-Switchable Fluorescence, *Adv. Mater.*, 2024, **11**, 2401325.
18. Z.-P. Zhang, X. Liu, X. Liu, Z.-W. Lu, X. Sui, B.-Y. Zhen, Z. Lin, L. Chen and L.-M. Wu, Driving Nonlinear

- Optical Activity with Dipolar 2-Aminopyrimidinium Cations in $(C_4H_6N_3)^+(H_2PO_3)^-$, *Chem. Mater.*, 2022, **34**, 1976-1984.
19. D.-X. Yang, Y.-L. Lv, J.-D. Guo, W.-Y. Gao, W. Liu and R.-L. Tang, From $(C_6H_5N_2)_2CdCl_4$ to $(C_6H_5N_2)_2ZnCl_4$, Chirality Transformation to Realize a Nonlinear Optical Organic-Inorganic Hybrid Halide with Balanced Comprehensive Performance, *Inorg. Chem.*, 2025, **64**, 3643-3648.
20. H. T. Luo, T. Tkaczyk, E. L. Dereniak, K. Oka and R. Sampson, High birefringence of the yttrium vanadate crystal in the middle wavelength infrared, *Opt. Lett.*, 2006, **31**, 616-618.
21. M.-H. Lv, S.-F. Li, M.-M. Ren, J.-X. Wang, R.-L. Tang, J. Chen, H. Huang, B. Zhang and D. Yan, $[C(NH_2)_3]_6Mo_7O_{24}$: A Guanidinium Molybdate as a UV Nonlinear Optical Crystal with Large Birefringence, *Inorg. Chem.*, 2024, **63**, 3948-3954.
22. P. Zhang, X. Mao, X. Dong, L. Huang, L. Cao, D. Gao and G. Zou, Two UV organic-inorganic hybrid antimony-based materials with superior optical performance derived from cation-anion synergetic interactions, *Chin. Chem. Lett.*, 2024, **35**.
23. G. Ghosh, Dispersion-equation coefficients for the refractive index and birefringence of calcite and quartz crystals, *Opt. Commun.*, 1999, **163**, 95-102.
24. Y.-H. Wang, D.-X. Jiang, D.-X. Liu, F.-Y. Li, H. Zhao, J. Pan, Q. Wei, L. Wei and G.-Y. Yang, $(C_{10}N_2H_{10})(HI_2O_6)(HIO_3)(IO_3)$: A Birefringent Material Featuring Large π -Conjugated Organic Cation and Two Types of Iodate Anions, *Inorg. Chem.*, 2024, **63**, 20774-20780.
25. Z. Tang, H. Huang, Y. Zhou, Y. Wang, Y. Shen, R. Yan and L. Wu, $[C_8H_6BrN_2O]Cl$ and $[C_8H_6IN_2O]Cl$: Two birefringent crystals with π -conjugated quinazoline groups, *Inorg. Chem. Commun.*, 2024, **170**, 113178.
26. Y. Zhang, M.-H. Lv, S.-F. Li, H. Huang, B. Zhang and D. Yan, $[C(NH_2)_3]_{10}(MoO_3)_{10}(PO_4)_2(HPO_4)_{2-5}H_2O$: Synergy effect of multiple functional units results in significant birefringence, *J. Solid State Chem.*, 2024, **337**, 124823.
27. H.-L. Zhang, D.-X. Jiao, X.-F. Li, C. He, X.-M. Dong, K. Huang, J.-H. Li, X.-T. An, Q. Wei and G.-M. Wang, A Noncentrosymmetric Metal-Free Borophosphate: Achieving a Large Birefringence and Excellent Stability by Covalent-Linkage, *Small*, 2024, **20**, 2401464.
28. X. Dong, Y. Long, L. Huang, L. Cao, D. Gao, J. Bi and G. Zou, Large optical anisotropy differentiation induced by the anion-directed regulation of structures, *Inorg. Chem. Front.*, 2022, **9**, 6441-6447.
29. S. Li, D. Dou, C. Chen, Q. Shi, B. Zhang and Y. Wang, $[C(NH_2)_3]_2S_2O_6$: A SBBO-Like Dithionate Crystal with Large Optical Anisotropy, *Inorg. Chem.*, 2024, **63**, 24076-24082.
30. X. Dong, Z. Zhang, L. Huang and G. Zou, $[C(NH_2)_3]BiCl_2SO_4$: an excellent birefringent material obtained by multifunctional group synergy, *Inorg. Chem. Front.*, 2022, **9**, 5572-5578.
31. Y. Chen, T. Zhu, Z. Xiong, Y. Zhou, Y. Li, Q. Ding, Y. Liu, X. Chen, S. Zhao and J. Luo, An organic-inorganic hybrid birefringent material with diverse functional groups, *Chem. Commun.*, 2021, **57**, 6668-6671.
32. Z. Guoqing, X. Jun, C. Xingda, Z. Heyu, W. Siting, X. Ke, D. Peizhen and G. Fuxi, Growth and spectrum of a novel birefringent α -BaB₂O₄ crystal, *J. Cryst. Growth*, 1998, **191**, 517-519.
33. F. Wu, Q. Wei, X. Li, Y. Liu, W. Huang, Q. Chen, B. Li, J. Luo and X. Liu, Cooperative Enhancement of Second Harmonic Generation in an Organic-Inorganic Hybrid Antimony Halide, *Cryst. Growth Des.*, 2022, **22**, 3875-3881.
34. Y. Shen, W. Niu, Y. Luo, Y. Zhou, X. Xue and L. Liu, $(C_8H_6BrN_2O)NO_3$: A Hybrid Nonlinear Optical Crystal With an Appropriate Birefringence, *Adv. Optical Mater.*, 2024, **12**, 2400062.
35. D. E. Zelmon, D. L. Small and D. Jundt, Infrared corrected Sellmeier coefficients for congruently grown lithium niobate and 5 mol. % magnesium oxide-doped lithium niobate, *J. Opt. Soc. Am. B*, 1997, **14**, 3319-3322.